In situ "artificial plasma" calibration of tokamak magnetic sensors

D. Shiraki,[1] J. P. Levesque,[1] J. Bialek,[1] P. J. Byrne,[1] B. A. DeBono,[1] M. E. Mauel,[1] D. A. Maurer,[2] G. A. Navratil,[1] T. S. Pedersen,[3] and N. Rath[1]
[1]*Department of Applied Physics and Applied Mathematics, Columbia University, New York, New York 10027, USA*
[2]*Physics Department, Auburn University, Auburn, Alabama 36849, USA*
[3]*Max Planck Institute for Plasma Physics, EURATOM Association, Wendelsteinstr. 1, 17491 Greifswald, Germany*

(Received 21 November 2012; accepted 20 May 2013; published online 7 June 2013)

A unique *in situ* calibration technique has been used to spatially calibrate and characterize the extensive new magnetic diagnostic set and close-fitting conducting wall of the High Beta Tokamak-Extended Pulse (HBT-EP) experiment. A new set of 216 Mirnov coils has recently been installed inside the vacuum chamber of the device for high-resolution measurements of magnetohydrodynamic phenomena including the effects of eddy currents in the nearby conducting wall. The spatial positions of these sensors are calibrated by energizing several large *in situ* calibration coils in turn, and using measurements of the magnetic fields produced by the various coils to solve for each sensor's position. Since the calibration coils are built near the nominal location of the plasma current centroid, the technique is referred to as an "artificial plasma" calibration. The fitting procedure for the sensor positions is described, and results of the spatial calibration are compared with those based on metrology. The time response of the sensors is compared with the evolution of the artificial plasma current to deduce the eddy current contribution to each signal. This is compared with simulations using the VALEN electromagnetic code, and the modeled copper thickness profiles of the HBT-EP conducting wall are adjusted to better match experimental measurements of the eddy current decay. Finally, the multiple coils of the artificial plasma system are also used to directly calibrate a non-uniformly wound Fourier Rogowski coil on HBT-EP. © *2013 AIP Publishing LLC*. [http://dx.doi.org/10.1063/1.4808366]

I. INTRODUCTION

Magnetic diagnostics[1] are used in a variety of fusion relevant plasma devices.[2–5] These are essential for the purposes of equilibrium reconstruction[6,7] as well as instability and mode detection.[4] Since both processes require accurate measurements of the spatial structure of the magnetic field, the physical locations of each sensor must be precisely known along with its sensitivity. Many such sensors measure the component of the magnetic field in a certain direction, making the orientation of these probes also important. In addition, magnetic diagnostics in many devices are heavily affected by eddy currents in surrounding conducting structures. Each of these factors must be understood for accurate interpretation of magnetic measurements.

The sensitivities of magnetic sensors are often calibrated on the bench, but can be determined *in situ* as well. Some *in situ* calibrations of the dc gain and frequency response of magnetic sensors rely only on the sensors and their corresponding cabling and circuitry.[2] Other works have used *in situ* measurements of sensor couplings to various calibration coils which are installed on the machine to determine sensitivities. Often such calibration coils are themselves part of the device, such as the poloidal field coils of a tokamak.[2,8] Dedicated *in situ* coils which simulate the plasma current are likely to have better coupling to sensors, and such coils have been built for calibrations of the sensitivities of installed Rogowski coils.[4,9] Such Rogowski coil calibrations depend only on the total enclosed current, and therefore do not require accurate construction and alignment of the calibration coil.

While the gains/sensitivities of magnetic sensors are commonly calibrated, the spatial positions of such sensors are not. For example, Ref. 8 measures the effective coupling between sensors and poloidal field coils in a tokamak, which thus includes the effects of sensor misalignments, but does not solve for them explicitly. In the absence of other techniques, determining the spatial positions of installed sensors may require detailed metrology work, which may be costly and time-consuming if the number of sensors is large. However, an alternative technique, introduced in Ref. 10, is to use magnetic measurements of individually energized equilibrium coils to infer the spatial positions of sensors.

In this paper, we present a variation of this *in situ* calibration technique for the final positions of installed magnetic sensors in the High Beta Tokamak-Extended Pulse (HBT-EP) experiment,[11] based on magnetic measurements using a dedicated set of *in situ* calibration coils, which were temporarily installed during an up-to-air period. Based on the measured coupling between a sensor and the carefully aligned set of calibration coils, the positions of the various sensors can be deduced. Since the calibration coils are built near the nominal location of the plasma current centroid, the technique is referred to as an "artificial plasma" calibration. In contrast to the artificial plasma coils used in Ref. 4 or 9, the design of the artificial plasma on HBT-EP includes multiple coils which may be individually energized, in order to determine the spatial positions of the sensors. In addition, the techniques described

here allow characterization of the electromagnetic properties of nearby conducting structures and their effects on magnetic diagnostics.

The remainder of the paper is organized as follows. Section II describes the new magnetic diagnostic set and conducting wall of the HBT-EP device. Section III describes the artificial plasma coil system. Section IV gives an overview of analysis methods. Section V compares measured sensor-coil couplings with those predicted by metrology data. Section VI describes the fitting of sensor positions based on magnetic measurements. Section VII compares results with simulations using the VALEN code to characterize the conducting wall of HBT-EP. Section VIII describes the calibration of a Fourier Rogowski coil using the artificial plasma. Finally, Sec. IX gives the conclusions.

II. HBT-EP DEVICE AND MAGNETICS

The HBT-EP experiment studies the physics and control of beta-limiting magnetohydrodynamic (MHD) instabilities such as the resistive wall mode (RWM).[12–14] The RWM is an ideal external kink mode whose growth rate has been slowed to a magnetic diffusion time set by the presence of a nearby conducting wall. Thus, HBT-EP has a close-fitting conducting wall near the plasma boundary, which has recently been upgraded.[15] The wall is made of 20 independent segments (Fig. 1), which can be individually moved in the minor radius direction to vary the plasma-wall coupling. Each wall segment is constructed of 0.48 cm thick 316 stainless steel, with a 127 μm electroplated layer of copper and a 7.6 μm coating of chrome. The purpose of the copper is to adjust the L/R diffusive wall time which sets the RWM growth rate, while the chrome reduces the sputtering of copper in the scrape-off layer plasma. Although the design value of the copper plating was a uniform thickness of 127 μm, it is known from bench electromagnetic as well as optical microscope measurements that there is significant variation in the thickness of the copper plating across the 20 wall segments, with the general trend being that there is excess copper on most segments. These electromagnetic measurements of relative copper thicknesses between wall segments were based on the measured effective inductance of a nearby coil. Also, micrometer and microscope measurements indicate that there is more copper near the edge of each wall segment, giving a "hollow" profile to the copper thickness, rather than the uniform thickness as designed.

FIG. 1. The close-fitting conducting wall of the HBT-EP device. The wall is composed of 20 individual stainless steel segments, each of which is coated in copper to adjust the L/R time of the wall. Copper thicknesses shown here are based on the modeling discussed in Sec. VII.

Mounted on these wall segments as well as on other internal structures are the magnetic sensors themselves, which are Mirnov coils[1] oriented to measure the radial and poloidal components of the equilibrium and fluctuating fields. Construction of the sensors consists of 10–20 turns of 30 AWG Kapton wire wound around a machined Teflon form. The Teflon forms are of two types, with large (106 mm × 20 mm) "feedback" sensors and small (26 mm × 15 mm) "high-density" sensors. Both types of sensors have windings for radial and poloidal field measurements. All sensors are partially integrated by an analog integrator, with numerical correction for the finite RC times. Since over half of the magnetic sensors are directly mounted on the conducting wall, eddy current effects are significant in these sensor signals. The distribution of sensors within the machine is fully described in Ref. 15.

The NA (turns × cross-sectional area) of each sensor is bench calibrated using a large Helmholtz coil. The ultimate limit on the accuracy of the calibration is set by deformation of the sensor itself.[16] To quantify this, each sensor was calibrated three or more times, to give a range of measured NAs. Depending on sensor type, the median spread in measured NA was up to 0.46%, with a maximum spread of 1.9%.

III. ARTIFICIAL PLASMA CONSTRUCTION

The HBT-EP artificial plasma system consists of four independent single-turn coils of 0.64 cm diameter copper rod. Three of the coils are positioned at the machine midplane. One of these has a major radius of 92 cm to match the nominal plasma major radius, with the other coils shifted at ±2.5 cm. The fourth coil also has 92 cm major radius and is located 1.9 cm below the midplane. This configuration as installed is shown in Fig. 2. The coils are mounted in a G10 structure which is supported off of the close-fitting conducting wall. Construction of all four coils in a single fixed structure allows installation and alignment of all of the coils simultaneously. The artificial plasma assembly is built in eight toroidal segments to allow installation through the vacuum chamber ports.

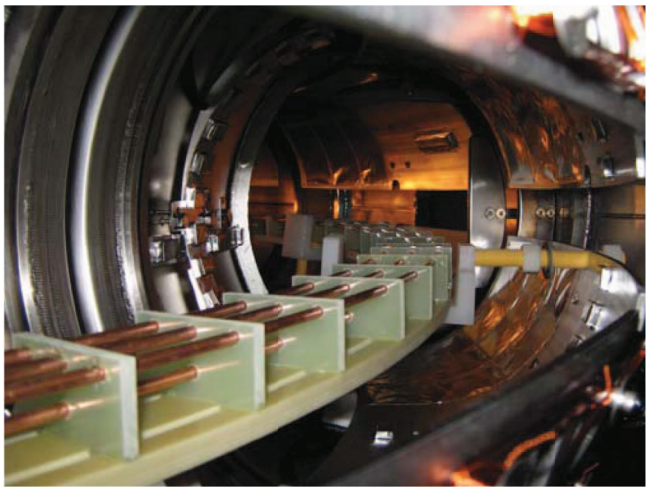

FIG. 2. Artificial plasma coils in the HBT-EP vacuum chamber. The conducting wall segments have been pulled back in this picture, but were in their fully inserted positions during the artificial plasma experiments.

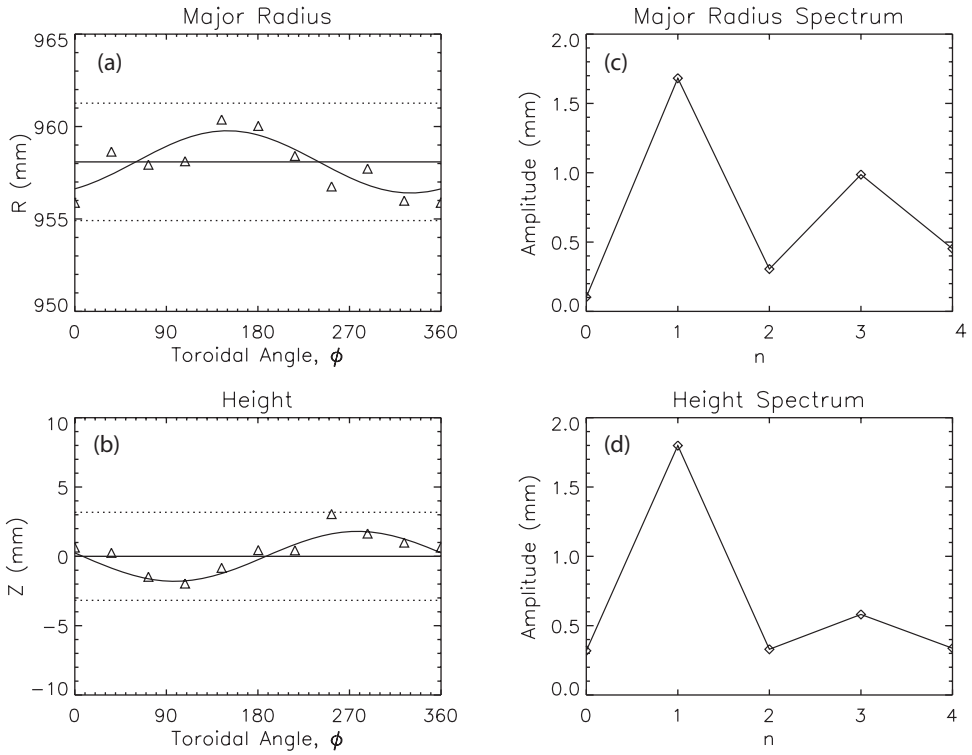

FIG. 3. (a) and (b) Measured alignment of artificial plasma assembly, along with the best-fit $n = 1$ component. The dashed lines represent the physical dimensions of the copper conductor itself. (c) and (d) Fourier decomposition shows that the major deviations are $n = 1$, corresponding to a shift and a tilt.

The radial and vertical alignment of the artificial plasma was measured to be within 3 mm of the design, which is less than the minor radius of the copper conductor. The dominant alignment errors are $n = 1$, as shown in Fig. 3, corresponding to a shift and a tilt of the assembled artificial plasma coils.

The coils are energized individually with a capacitor bank consisting of a 25 kV, 60 μF start bank and a 450 V, 0.25 F power-crowbar bank to produce a step-like waveform. Currents up to 5 kA were driven in the artificial plasma. In comparison, the plasma currents of HBT-EP plasmas are of order 15 kA.

IV. ANALYSIS

The signal s in a given magnetic sensor can be related to the current I in a calibration coil of major radius R_i by a response function[8]:

$$s(t, R_i) = \int_0^t \frac{dI}{d\tau} \cdot r(t - \tau; R_i) d\tau. \quad (1)$$

The response function r can be found by deconvolution. It represents the sensor response to a perfect step-function applied to the coil, as seen by substitution of a step-function for $I(\tau)$ in Eq. (1). Several examples of measured response functions on HBT-EP are shown in Fig. 4. In the absence of eddy currents in nearby conducting structures, the response function itself is a step-function with height equal to the time-independent Green's function for the particular coil-sensor pair. If eddy currents are present, the response function will differ from a step-function due to the fields created by the eddy currents. As these eddy currents decay, the response function approaches the vacuum response, so that the asymptotic value equals the time-independent Green's function:

$$G_{meas}(R_i) = \lim_{t \to \infty} r(t; R_i). \quad (2)$$

This experimentally measured Green's function, which has units of G/kA, is the vacuum coupling between this particular sensor and coil. We can also compute this value if we know the exact position of the sensor:

$$G(\rho, \theta; \xi_1, \xi_2, R_i) = \frac{\vec{B}(\rho, \theta; I, R_i) \cdot \hat{n}(\xi_1, \xi_2)}{I}, \quad (3)$$

where the position of the sensor is described in toroidal coordinates (ρ, θ, ϕ), and the orientation of the sensor is parameterized by two Euler angles (ξ_1, ξ_2) which describe rotations about the directions of the machine axis and the local magnetic axis, respectively. Here, the coordinates of the source, other than the major radius, are not written explicitly. The Green's function is independent of ϕ due to the assumed axisymmetry of the artificial plasma coils.

As mentioned, the difference between the response function and a step-function gives the eddy current contribution to the sensor signal. As the eddy currents decay, this difference goes to zero and the response function asymptotes to the value of the vacuum coupling. We can fit one or several time-constants to this response function decay. With the artificial plasma coils in HBT-EP, this decay is well-represented with a single exponential decay rate.

The response function r has been found by deconvolution, based on a known sensor signal and artificial plasma current. Conversely, the validity of a given response function can be tested by substitution in Eq. (1) along with a known

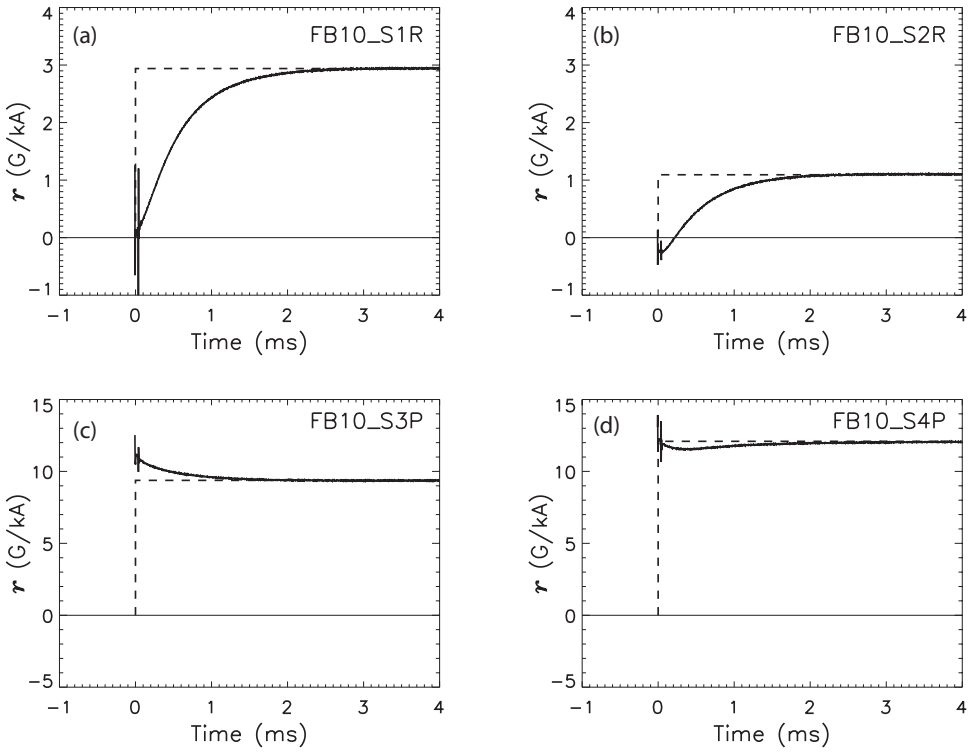

FIG. 4. Examples of HBT-EP response functions for the artificial plasma located at $R = 92$ cm and $z = 0$. Also shown (dashed) are the ideal step responses which would be seen in the absence of eddy currents. Examples shown include (a) and (b) radial field sensors, and (c) and (d) poloidal field sensors.

current $I(t)$, which need not be the one originally used to calculate the response function.[8] This convolution then predicts the sensor signal which should be measured. Such a comparison is shown in Fig. 5, where the predicted signal due to a rapidly oscillating 4.1 kHz current in the artificial plasma is compared with the measured signal. The response function is seen to accurately capture the effects of eddy currents in the HBT-EP conducting wall. This response function technique will be used throughout the paper to measure the vacuum sensor-coil couplings (Eq. (2)), for comparison with calculations of the expected coupling based on possible sensor coordinates (Eq. (3)). In addition, the decay of the response function will be used in Sec. VII to characterize the electromagnetic properties of the conducting wall.

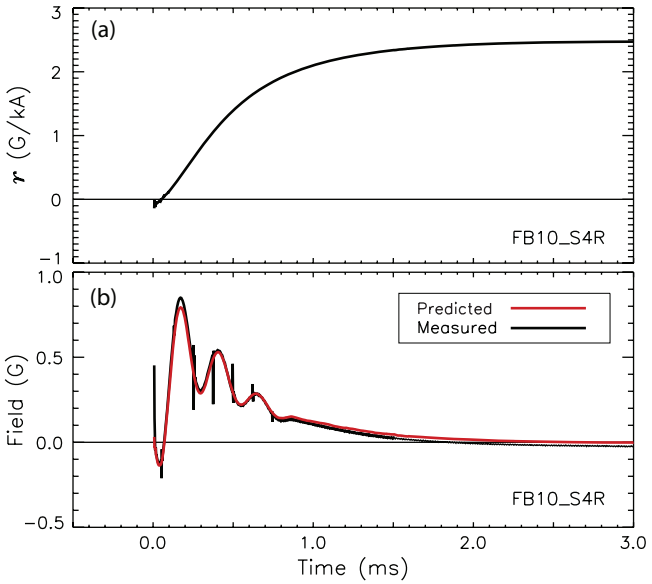

FIG. 5. (a) Response function for a radial field sensor and the artificial plasma at $R = 92$ cm, $z = 0$. (b) Comparison of the predicted and measured signal due to a 4.1 kHz oscillating artificial plasma current, for the same sensor. The predicted signal is a convolution of the response function shown in (a) with the oscillating artificial plasma current (Eq. (1)).

V. COMPARISON TO METROLOGY

The geometry of the new conducting wall and magnetic sensors were measured with ROMER and FARO coordinate measuring machines (CMMs).[17] First, a ROMER INFINITE portable measuring arm was used to measure sensors and conducting wall segments as assembled on the bench. After the wall segments were installed in the vacuum vessel, a laser tracker manufactured by FARO Technologies established a global toroidal coordinate system based on toroidal field magnet locations. Finally, the ROMER CMM was used to measure locations and orientations of the wall segments *in situ* with respect to the established coordinate system. Absolute sensor positions were measured to ~1.0 mm accuracy.

With the measured positions of the artificial plasma coils as well as the known spatial structure of the resulting dipole field, the expected Green's functions for all sensor-coil pairs can be calculated using the measured sensor positions in Eq. (3). These Green's functions are shown in Fig. 6, along with the same values calculated using the nominal sensor coordinates, as well as the measured values from the response function technique. Because the design of the machine is

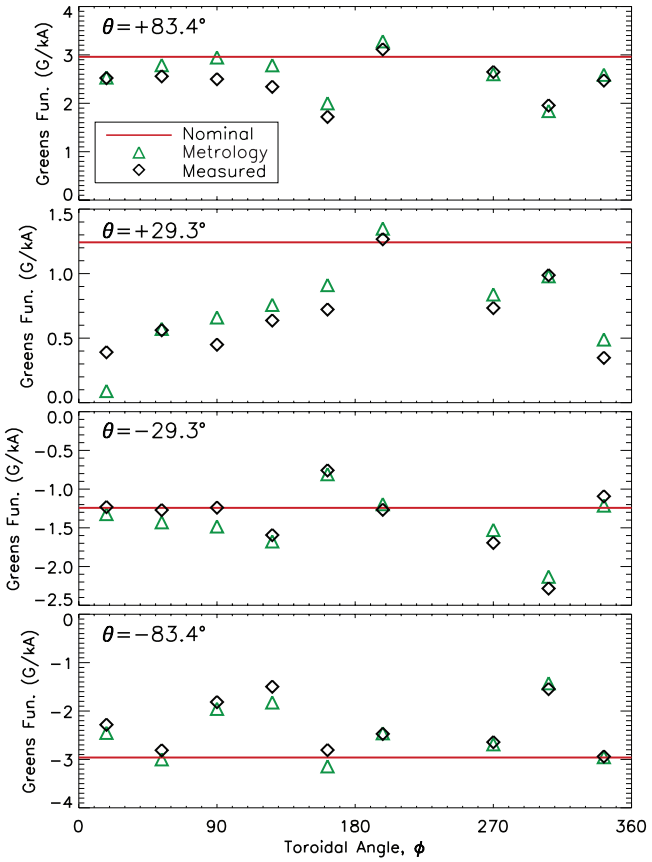

FIG. 6. Comparison of experimentally measured Green's functions with values calculated using nominal and metrology-based sensor coordinates, for the $R = 92$ cm, $z = 0$ artificial plasma. Green's functions are negative for sensors below the midplane ($\theta < 0$), with zero at the top of the y-axis.

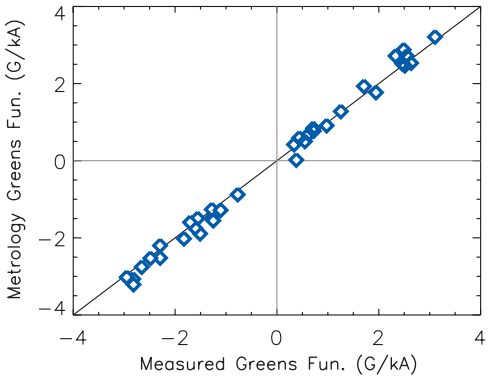

FIG. 7. Comparison of Green's functions measured using the response function technique (Eq. (2)) on the x-axis, with those calculated using metrology-based sensor coordinates (Eq. (3)) on the y-axis, for the $R = 92$ cm, $z = 0$ artificial plasma. The 1-1 line between the two methods is also shown.

nominally axisymmetric, those values calculated using nominal sensor coordinates are independent of the toroidal angle ϕ. If sensor misalignments are accounted for by using the metrology-based coordinates in Eq. (3), the Green's functions are seen to differ significantly from the nominal values. These calculated deviations are due to the individual errors in sensor positions, giving each sensor a different coupling to the same artificial plasma.

The experimental measurements of the Green's functions also vary from the nominal values, and these deviations from the nominal values are seen to correlate well with those of the metrology-based results. This overall agreement between the two methods of determining the Green's functions (Eqs. (2) and (3)) is shown in Fig. 7. The standard deviation between the two methods is 0.16 G/kA with a maximum difference of 0.47 G/kA. The agreement between the two methods demonstrates that the differences between the measured sensor-coil couplings and their nominal values are due to the errors in the positions of the sensors, which have been measured by metrology.

VI. FITTING FOR SENSOR POSITIONS

In Sec. V, it was shown that the measured coupling of a sensor to a single artificial plasma coil can be understood by considering the actual position of the sensor, including errors relative to the nominal position. This allows the positional errors of a sensor to be inferred given a sufficient number of such magnetic measurements. Because the artificial plasma system in HBT-EP contains multiple independent coils, the coupling of a sensor to each of these coils can be measured independently, allowing that sensor's actual position to be deduced by fitting to these measurements. This fit of the sensor's position offers an improvement to the nominal spatial coordinates of the sensor, and represents the final installed position of the sensor, as determined by these *in situ* measurements. This is similar to the principle of "magnetic triangulation" discussed in Ref. 2.

The fit for a sensor's position is accomplished by fixing the bench calibrated *NA* value and taking the Green's function to be only a function of the sensor's location and orientation. This can be parameterized by five variables: three spatial coordinates and two Euler angles. Because the artificial plasmas are toroidally symmetric, we are unable to resolve the ϕ coordinate from any measurements. Since we have four independent artificial plasma coils, it should be possible in principle to fit the remaining four unknowns. Data are available for only the three artificial plasmas at the machine midplane, so here we take the metrology-based Euler angles (ξ_1, ξ_2) to be correct, and only fit for the spatial coordinates (ρ, θ), leaving a two parameter fit to the three measurements.

Thus, for each sensor, we minimize in a least-squares sense the residual between measured and computed Green's functions for the three artificial plasmas:

$$E(\rho,\theta) = \left[\sum_i \left(G_{meas}(R_i) - G(\rho,\theta;\xi_1,\xi_2,R_i)\right)^2\right]^{1/2}. \tag{4}$$

Figure 8 shows contours of this residual as a function of possible sensor coordinates, for four radial feedback sensors. The "best-fit" coordinates in this method are defined as those which minimize the total residual. This fitting shows that adjustments of the sensor position from their nominal values result in a better overall agreement with the measured couplings to the multiple artificial plasmas. The corrections to

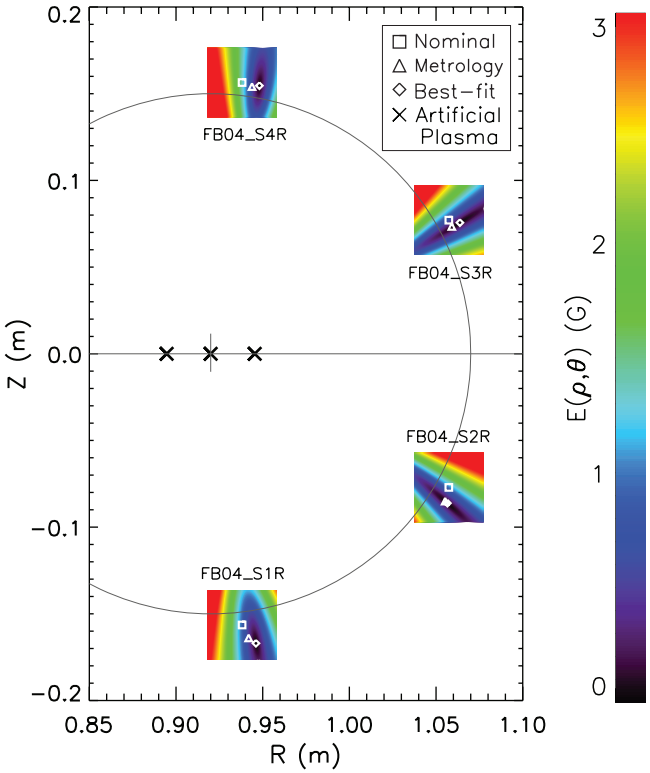

FIG. 8. Contours of the residual between experimentally measured Green's functions and those calculated as a function of possible sensor coordinates, as defined in Eq. (4), for four individual sensors. The toroidal coordinates (ρ, θ) are defined about $R = 0.92$ m, $z = 0$. The nominal, metrology, and best-fit coordinates for each sensor are shown, along with the locations of the artificial plasmas.

the nominal coordinates of each sensor are seen to be in rough agreement with the results of metrology, with the maximum distance between artificial plasma and metrology-based coordinates being 5.2 mm. This level of fitting is based only on the measured couplings to three artificial plasma coils whose locations are shown in Fig. 8. The addition of more constraints by constructing additional calibration coils would allow further refinements of this fit. The contours in Fig. 8 show that these particular measurements are relatively insensitive to positional errors in the minor radial direction. This is due to all three artificial plasmas being relatively close to the toroidal axis at $R = 0.92$ cm. Additional calibration coils off of the midplane ($z = 0$), for example, could help to further resolve errors in these directions.

The improvement in matching the experimentally measured couplings to the multiple artificial plasmas is shown again in Fig. 9, where expected Green's functions are plotted as a function of artificial plasma radius. Three curves are shown using the nominal, metrology, and best-fit sensor coordinates, respectively, along with the measured Green's functions for the three artificial plasmas. Again, adjustments of the sensor coordinates from their nominal values improve agreement between expected and measured Green's functions.

VII. VALEN MODELING

In Secs. V and VI, we have described the vacuum coupling between the sensors and the artificial plasma coils, which depends only on sensor/coil geometries and is not

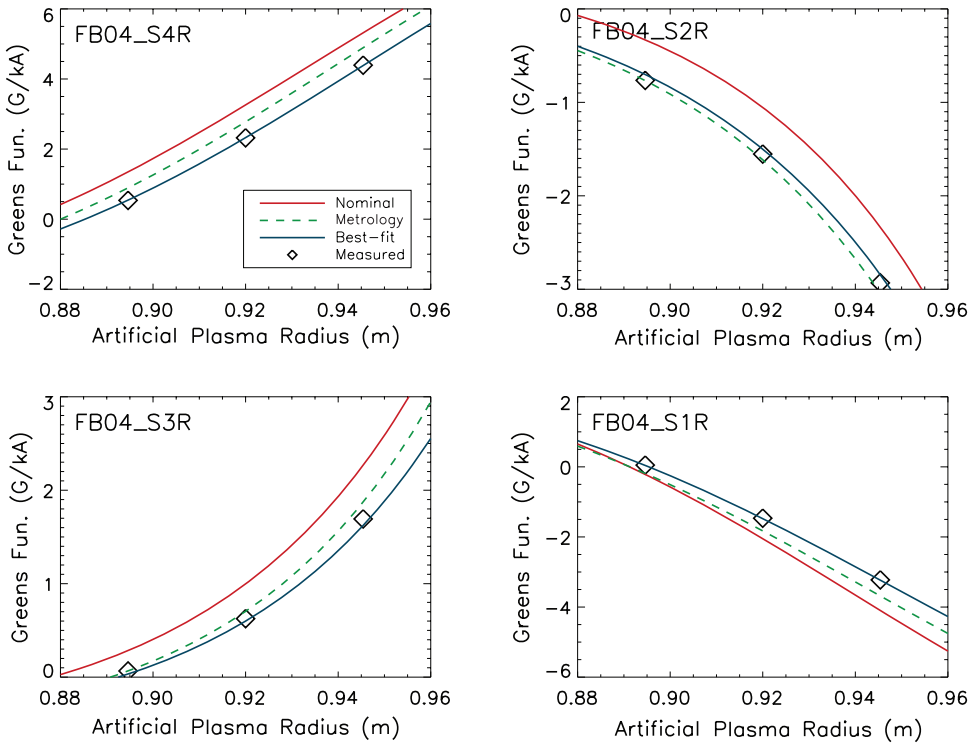

FIG. 9. Comparison of measured Green's functions with calculated Green's functions using nominal, metrology, and best-fit sensor coordinates, as a function of artificial plasma radius.

affected by the presence of the nearby conducting wall. The experimentally measured response functions reach this asymptotic vacuum value only after several eddy current decay times. We now consider the rate at which this decay occurs, which is dependent on the details of the conducting structures in the device. This is compared with modeling of the artificial plasma experiment using the finite-element electromagnetic code VALEN,[18] in order to characterize the electromagnetic properties of the conducting wall in HBT-EP. VALEN contains a detailed three-dimensional model of the close-fitting conducting wall in HBT-EP, and is used to simulate a variety of RWM feedback experiments carried out on the device.[12,19,20]

Using the experimentally measured artificial plasma current trace, we run a time-domain calculation to compute the expected eddy currents in the surrounding conducting wall. From this simulation, we can calculate the response function for each coil/sensor pair, and all resulting values such as the vacuum Green's function or response function decay time. For this simulation, we use the nominal locations and orientations of the sensors. Comparing with experiment, we find that the measured response function decay times differ systematically from the nominal values predicted by VALEN, with most of the measured values tending to be higher. This is in agreement with the microscope measurements indicating excess copper plating on the stainless steel wall, above the design values.

By varying the copper thickness profiles of the wall segments in the VALEN model, we are able to more closely match the measured response function decays. This is highlighted for a few sensors in Fig. 10. In particular, the decay time in the poloidal sensors is predicted to be higher near the midplane ($\theta = 0^\circ$), whereas the experimental measurements are clearly lower there. This feature is only recreated when the modeled copper thickness profile is made hollow, with more copper at the edges of the wall segments. In addition, both the radial and poloidal decay times measured tend to be systematically higher or lower for different segments of the wall. This was adjusted by changing the total amount of copper on each individual wall segment in the model. The final model for the copper thickness on the HBT-EP conducting wall is shown in Fig. 1. The adjustments made here (both in total copper and in the thickness profiles across each segment) were found to be consistent with the bench electromagnetic, microscope, and micrometer measurements of relative copper thicknesses between wall segments, which were discussed in Sec. II.

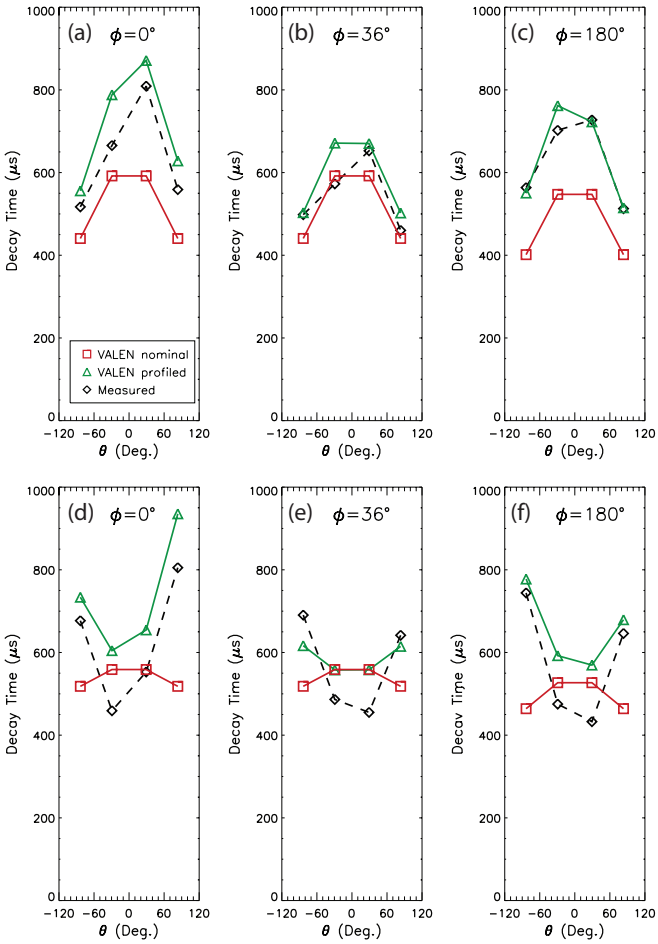

FIG. 10. Comparison of measured and VALEN modeled response function decay times, for several feedback sensors. VALEN results are shown for two cases: with nominal uniform copper plating of wall segments, and with adjusted copper profiles to better match the measured values. Examples shown include (a)–(c) radial field sensors and (d)–(f) poloidal field sensors.

VIII. FOURIER ROGOWSKI CALIBRATION

The design of the artificial plasma on HBT-EP, with its multiple independent coils of different major radii, allows a straightforward calibration of Rogowski coils of non-uniform winding density. The major radial position of HBT-EP plasmas is computed based on a Rogowski coil with spatial winding density proportional to $\cos(\theta)$, which detects the poloidal mode number $m = 1$ cosine component of the poloidal field. This Fourier Rogowski coil has previously been calibrated in actual plasma discharges, using a movable array of internal magnetic probes to detect the poloidal field null at the plasma current centroid.[21] The artificial plasma allows a far simpler and more reliable calibration of this Fourier Rowgowski coil, due to its multiple coils of known major radius. By energizing each of these coils in turn, the $m = 1$ Rogowski signal as a function of the major radius of the current centroid is directly calibrated.

The result of this Fourier Rogowski calibration has been verified in actual plasma discharges, based on detection of the plasma edge. HBT-EP contains multiple sets of limiters, such that the actual limiting surface depends on the major radius of the plasma. Since the plasma boundary is determined by the limiting surface and the positions of the limiters have been measured, the location of the plasma boundary can be calculated as a function of the major radius, which is measured using the Fourier Rogowski coil. We compare this with detection of the plasma edge using a grounded Langmuir probe which draws current only when it is inside the last closed flux surface, and no longer conducts once it leaves the plasma boundary. Figure 11 shows the evolution of the plasma edge for four discharges, as calculated from the Fourier Rogowski signal. In each of the discharges, at the times when the grounded Langmuir probe is calculated to leave the plasma edge, the current drawn through the probe is observed to fall

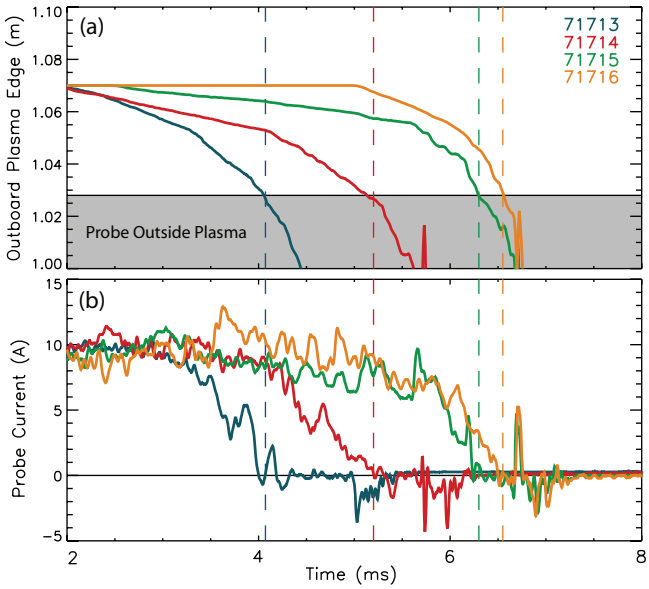

FIG. 11. (a) Location of the outboard plasma edge as a function of time for four HBT-EP plasma discharges, as calculated from the measured major radius. When the location of the plasma edge is less than 1.028 m, the grounded Langmuir probe is outside the plasma. (b) Current drawn through Langmuir probe.

to zero, verifying the artificial plasma calibration of the $m = 1$ Fourier Rogowski coil.

IX. CONCLUSIONS

The artificial plasma system implemented on HBT-EP consists of multiple independently energized calibration coils which were carefully constructed and installed in the experiment during an up-to-air period. This technique is used for a detailed *in situ* calibration of the spatial positions of a new set of magnetic diagnostics. This is achieved by fitting the measurements of sensor couplings to multiple calibration coils in order to determine the sensor positions and their deviations from their nominal coordinates. Metrology verifies that the unique values of the sensor-coil couplings measured using the response function technique are due to positional errors of the sensors, allowing a sensor's position to be determined from such magnetic measurements. In addition, measurements of the eddy current contribution to magnetic signals are used to improve the VALEN model of the HBT-EP conducting wall through adjustments of the modeled copper plating on the wall. Finally, the use of multiple artificial plasmas allows the direct *in situ* calibration of a Fourier Rogowski coil of non-uniform winding density.

The techniques described here may be relevant to devices with large diagnostic sets such as ITER[22] or to long-pulse devices such as W7-X[5] where eddy current effects will be significant, due to the need for in-vessel active cooling components with high thermal and electrical conductivity and non-trivial geometries. The implementation of an artificial plasma system on such future devices can be optimized in several manners. As discussed in Sec. VI, the measurement of a sensor's coupling to each additional artificial plasma coil provides another constraint on that sensor's position. Thus, an artificial plasma system designed with a large number of independent coils will result in an improved spatial calibration. This can potentially be augmented by combining this approach with the use of poloidal field coils as calibration coils (as in Ref. 8), provided their geometry and alignment are known with sufficient accuracy. The addition of calibration coils which break the toroidal symmetry of the system will allow the toroidal position of a sensor to be fit as well. The existing toroidal field coils of the device could be used for this, if they can be individually energized and if their geometry is well known. Given a sufficient number of calibration coils, an artificial plasma calibration could potentially be used in place of detailed metrology of the sensors, which may be costly and time-consuming for large diagnostic sets. Of course, the technique requires accurate alignment of the calibration coil itself, so that metrology cannot be avoided entirely. However, this process is potentially much simpler than the detailed measurement of a large set of individual sensors, particularly if the artificial plasma coils are assembled as a single unit which can be simultaneously aligned, as in the design used on HBT-EP. Furthermore, magnetic sensors may be located behind other structures in the experiment which may limit access and prevent direct measurement of sensor positions by metrology. In such cases, the alignment of a single artificial plasma system near the center of the vessel volume may be preferable.

ACKNOWLEDGMENTS

The authors would like to thank Steve Raftopoulos of Princeton Plasma Physics Laboratory for his metrology work. The authors also thank Nick Rivera and Jim Andrello for their technical assistance with the project. This work was supported by U.S. Department of Energy Grant DE-FG02-86ER53222.

[1] I. Hutchinson, *Principles of Plasma Diagnostics* (Cambridge University Press, 2005).
[2] J.-M. Moret, F. Buhlmann, D. Fasel, F. Hofmann, and G. Tonetti, Rev. Sci. Instrum. **69**, 2333 (1998).
[3] V. Coccorese, R. Albanese, H. Altmann, S. Cramp, T. Edlington, K. Fullard, S. Gerasimov, S. Huntley, N. Lam, A. Loving, V. Riccardo, F. Sartori, C. Marren, E. McCarron, C. Sowden, J. Tidmarsh, F. Basso, A. Cenedese, G. Chitarin, F. Degli Agostini, L. Grando, D. Marcuzzi, S. Peruzzo, N. Pomaro, and E. R. Solano, Rev. Sci. Instrum. **75**, 4311 (2004).
[4] E. J. Strait, Rev. Sci. Instrum. **77**, 023502 (2006).
[5] J. Geiger, M. Endler, and A. Werner, Contrib. Plasma Phys. **50**, 736 (2010).
[6] J. Luxon and B. Brown, Nucl. Fusion **22**, 813 (1982).
[7] L. Lao, H. S. John, R. Stambaugh, A. Kellman, and W. Pfeiffer, Nucl. Fusion **25**, 1611 (1985).
[8] J. Spaleta, L. Zakharov, R. Kaita, R. Majeski, and T. Gray, Rev. Sci. Instrum. **77**, 10E305 (2006).
[9] S. G. Lee and J. G. Bak, in *34th EPS Conference on Plasma Physics* (European Physical Society, 2007), Vol. 31F, paper. P5.102.
[10] F. Piras, J.-M. Moret, and J. Rossel, Fusion Eng. Des. **85**, 739 (2010).
[11] G. A. Navratil, C. Cates, M. E. Mauel, D. Maurer, D. Nadle, E. Taylor, Q. Xiao, W. A. Reass, and G. A. Wurden, Phys. Plasmas **5**, 1855 (1998).
[12] C. Cates, M. Shilov, M. E. Mauel, G. A. Navratil, D. Maurer, S. Mukherjee, D. Nadle, J. Bialek, and A. Boozer, Phys. Plasmas **7**, 3133 (2000).
[13] M. Shilov, C. Cates, R. James, A. Klein, O. Katsuro-Hopkins, Y. Liu, M. E. Mauel, D. A. Maurer, G. A. Navratil, T. S. Pedersen, N. Stillits, R. Fitzpatrick, and S. F. Paul, Phys. Plasmas **11**, 2573 (2004).
[14] J. M. Hanson, B. D. Bono, R. W. James, J. P. Levesque, M. E. Mauel, D. A. Maurer, G. A. Navratil, T. S. Pedersen, and D. Shiraki, Phys. Plasmas **15**, 080704 (2008).

[15]D. A. Maurer, J. Bialek, P. J. Byrne, B. D. Bono, J. P. Levesque, B. Q. Li, M. E. Mauel, G. A. Navratil, T. S. Pedersen, N. Rath, and D. Shiraki, Plasma Phys. Controlled Fusion **53**, 074016 (2011).
[16]D. Shiraki, Ph.D. dissertation, Columbia University, 2012.
[17]J. P. Levesque, P. J. Byrne, B. DeBono, B. Li, M. E. Mauel, D. A. Maurer, G. A. Navratil, N. Rath, and D. Shiraki, Bull. Am. Phys. Soc. **55**(15), GP9.00086 (2010).
[18]J. Bialek, A. H. Boozer, M. E. Mauel, and G. A. Navratil, Phys. Plasmas **8**, 2170 (2001).
[19]A. J. Klein, D. A. Maurer, T. S. Pedersen, M. E. Mauel, G. A. Navratil, C. Cates, M. Shilov, Y. Liu, N. Stillits, and J. Bialek, Phys. Plasmas **12**, 040703 (2005).
[20]M. Mauel, J. Bialek, A. Boozer, C. Cates, R. James, O. Katsuro-Hopkins, A. Klein, Y. Liu, D. Maurer, D. Maslovsky, G. Navratil, T. Pedersen, M. Shilov, and N. Stillits, Nucl. Fusion **45**, 285 (2005).
[21]D. Gates, Ph.D. dissertation, Columbia University, 1993.
[22]G. Vayakis and C. Walker, Rev. Sci. Instrum. **74**, 2409 (2003).